Study on Compression Induced Contrast in X-ray Mammograms Using Breast Mimicking Phantoms

A. B. M. Aowlad Hossain[1*], Min Hyoung Cho[2], Soo Yeol Lee[2]

[1]*Department of Electronics and Communication Engineering*
Khulna University of Engineering & Technology
Khulna-9203, Bangladesh
E-mail: aowlad0403@ece.kuet.ac.bd

[2]*Department of Biomedical Engineering*
Kyung Hee University
Youngin-si, Republic of Korea
E-mails: mhcho@khu.ac.kr, sylee01@khu.ac.kr

[*]*Corresponding author*

Received: April 13, 2015 **Accepted: September 23, 2015**

Published: September 30, 2015

Abstract: *X-ray mammography is commonly used to scan cancer or tumors in breast using low dose x-rays. But mammograms suffer from low contrast problem. The breast is compressed in mammography to reduce x-ray scattering effects. As tumors are stiffer than normal tissues, they undergo smaller deformation under compression. Therefore, image intensity at tumor region may change less than the background tissues. In this study, we try to find out compression induced contrast from multiple mammographic images of tumorous breast phantoms taken with different compressions. This is an extended work of our previous simulation study with experiment and more analysis. We have used FEM models for synthetic phantom and constructed a phantom using agar and n-propanol for simulation and experiment. The x-ray images of deformed phantoms have been obtained under three compression steps and a non-rigid registration technique has been applied to register these images. It is noticeably observed that the image intensity changes at tumor are less than those at surrounding which induce a detectable contrast. Addition of this compression induced contrast to the simulated and experimental images has improved their original contrast by a factor of about 1.4~2. We think the findings of this study will be helpful for clinical applications.*

Keywords: *Mammography, Contrast, Breast compression, Tissue elasticity, FEM modeling, Breast phantom.*

Introduction

Elastic properties of body tissues indicate their pathological as well as physiological states. It is well known that tissue stiffness plays an important role for the detection of tumor or cancerous tissues which are much harder than the surrounding normal tissues [13]. Elastography is an imaging method to envision the elasticity distribution in living tissues. Along with different elastography techniques, mainly ultrasound elastography and magnetic resonance elastography (MRE) are increasingly gaining their roles in the clinical applications. The basic principle is that, softer and harder tissues respond in a different way when subjected to external or internal mechanical forces. Elastic properties of tissues can be estimated qualitatively or quantitatively by analyzing the response. But, elastography images still suffer from low signal-to-noise ratio (SNR), poor spatial resolution and image artifacts.

X-ray mammography is widely used imaging modality with unparallel resolution even it can image the calcifications that related in the early stage of breast cancers [3, 4].

But, mammography suffers false diagnosis of low contrast lesions. Recently, the elastography concept has been applied to x-ray mammography and computed tomography to map elastic properties of breast tissues using elasticity theories [7, 8, 17]. These methods reconstructed 2D/3D images of tissue elastic properties directly or inversely using the deformation data from breast images under compressions as the usual procedure of elastography. But these methods require huge computations. In mammography, the breast is compressed in order to reduce the x-ray scattering effect. Due to the compression, the stiffer region inside the breast will be less deformed than the surrounding regions. The degree of deformation of breast tissues will be largely dependent on the force upon the compressing plate and importantly on the elasticity of the tissues. So, if two different compression level mammograms are taken then the compression, that is, elasticity related information can be incorporated with the original x-ray attenuation information to improve its contrast. In our previous simulation study [6], we have found that the x-ray image intensity changes at the tumor region are less than those at the nearby background region by factor of 0.66~0.84 for different compression levels. The strategic emphasis was that tissue's elastic contrast can be added to their x-ray attenuation contrast for improving the original contrast with less computation. Therefore, contrast can be improved keeping excellent resolution of mammogram whereas generally the resolutions of elastographic images are poor. This work is an experimental extension with more analysis initiated from the experience and motivation of our previous simulation study [6].

In this work, we try to enhance the contrast of mammogram using compression induced contrast from the multiple images of breast mimicking phantoms under different compression steps with typical mammography arrangements. This extra contrast can provide elastographic essence to mammography avoiding huge computational complexities. We plan to use breast mimicking 3D FEM model firstly to simulate breast with tumor inclusion considering tissue's elasticity properties to calculate the deformations. X-ray projection images under different levels of compression will be constructed assigning x-ray attenuation coefficient to FEM data. Then, we try to construct breast phantom with tumor using tissue mimicking chemicals and obtain experimental x-ray radiographs considering x-ray mammogram setup. An effective non-rigid registration technique is planned to apply on images of deformed phantom to match the images under different compressions for analyzing the pixel intensity changes at the tumor and the background. Finally, the impacts of compression induced contrast are examined and subsequently the issues raised are discussed and conclusions are drawn.

Materials and methods

Breast FE model and x-ray image simulation

When a deformable object is placed under compression, displacement field induced in it depending on the external pressures, boundary constraints and the mechanical properties. Continuum mechanics describes the deformation. Different mechanical breast models have been proposed considering linear or non-linear mechanics [1, 11, 15]. Soft tissues can be effectively modeled as linear elastic medium for small deformation. But when subjected to large compression, soft tissues undergo large recoverable elastic deformation which can be more accurately modeled by the nonlinear hyper-elasticity theory. That's why, in this work, we consider nonlinear modeling for mammographic compression. A nonlinear material cannot be described by a unique modulus; rather the modulus depends on applied strain and slope of the stress-strain curve. The deformation gradient used in the non-linear analysis, is a measure of changes in a body under external force [5].

The deformation gradient for a displaced position $\boldsymbol{x}$ from the reference position $\boldsymbol{X}$ can be expressed as, $\mathbf{F} = \partial \mathbf{x} / \partial \mathbf{X}$. Taking $\mathbf{B} = \mathbf{F} \cdot \mathbf{F}^{\mathrm{T}}$, the deformation invariants are defined as follows:

$$\begin{aligned} I_1 &= trace\left(\mathbf{B}\right) \\ I_2 &= \frac{1}{2}\left(I_1^{\,2} - trace\left(\mathbf{B}^2\right)\right) \\ I_3 &= \det\left(\mathbf{B}\right) \end{aligned} \tag{1}$$

where I_1, I_2, and I_3 are called the first, second, and third strain invariant of deformation, respectively.

Theory of hyperelasticity considers elastic material in which elastic parameters are characterized in terms of strain energy density function $W(I_1, I_2, I_3)$ defined from the deformation invariants.

A general polynomial form for strain energy density function is:

$$W = \sum_{i+j=1}^{N} C_{i,j} (\overline{I_1} - 3)^i (\overline{I_2} - 3)^j + \sum_{k=1}^{N} \frac{1}{d_k} (J_{el} - 1)^{2k} \tag{2}$$

where deviatoric invariants $\overline{I_p} = J_{el}^{\,-1/3} I_p$ for p = 1, 2, 3 and the elastic volumetric deformation ratio, $J_{el} = 1$ for incompressible material. $C_{i,j}$ and d_k are the hyperelastic parameters of the model.

Typically $C_{10} = \mu_0 / 2$, where μ_0 is initial shear modulus and $d_1 = 2 / k_0$, where k_0 is the initial bulk modulus.

The constitutive equation to describe the tissue deformation in terms of strain density function can be represented as [5]:

$$\boldsymbol{\sigma} = \frac{2}{\sqrt{I_3}} \left[\left(\frac{\partial W}{\partial I_1} + I_1 \frac{\partial W}{\partial I_2} \right) \mathbf{B} - \frac{\partial W}{\partial I_2} \mathbf{B} \cdot \mathbf{B} + I_3 \frac{\partial W}{\partial I_3} \mathbf{I} \right] \tag{3}$$

where $\boldsymbol{\sigma}$ is the stress tensor and $\mathbf{I}$ is the identity matrix. Finite element method can be used to calculate displacement using these stress-strain relationships that satisfy hyperelastic theory.

Though a real breast consists of many types of tissues such as fatty tissues, glandular ducts, and blood vessels, we have made simple breast FEM models having spherical tumors in the homogeneous background tissues to effectively observe the contrast changes in the tumor region. We have found from the literatures [9, 16] that the normal breast tissues have the Young's modulus of 2~5 kPa while tumor tissues have the value of 10~50 kPa under small deformation. But as the strain caused by the compression increases, the differences of elastic moduli of breast tissues also increase. At large deformation for mammographic imaging, Young's modulus of fatty tissue increases to about 30 kPa and for tumor tissues it increases to an order of hundreds kPa [9]. In this study, we chose the neo-Hookean hyperelastic material

with initial Young's modulus of 5 kPa and initial Poisson's ratio of 0.495 for the background. The breast model is hemi-elliptical shape with the size of 5×5×5 cm^3. To mimic tumor tissues, a homogeneous spherical inclusion of 8 mm diameter are placed on the center plane of the breast model as shown in Fig. 1. The center plane is normal to the compression direction. For the tumor mimicking inclusions, we use linear elastic material considering their relatively smaller strain due to higher stiffness. The Young's modulus and Poisson's ratio of the inclusion are 30 kPa and 0.495, respectively. We apply two strong flat compressing plates that can move vertically to mimic breast compression using sliding paddles in the mammography. For the FEM analysis, we used a commercial FEM package, ANSYS (ANSYS, Inc., Canonsburg, USA), to calculate displacement vectors inside the breast model under compression.

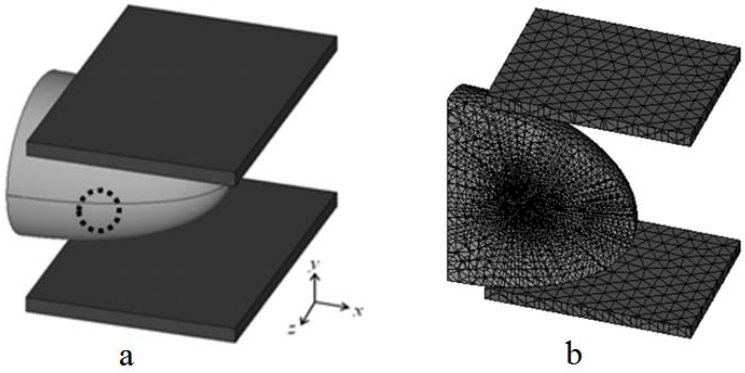

Fig. 1 The FE model of the breast:
a) breast model with the compressing plates, and b) its mesh diagram.
The left perpendicular plane of the breast model is a fixed plane mimicking
the connecting interface between the chest and breast.

In FEM analysis, we have to consider that the compressing plates give rise to a nonlinear contact problem between the soft breast surface and the much harder compressing plates. To make the breast model be only compressed without any deformation of the compressing plates, we set the Young's modulus, Poisson ratio and density to 200 GPa, 0.3 and 8000 kg/cm^3, respectively. This consideration assures virtually no deformation of the compressing plates. The model has been meshed into about 0.15 million elements including the contact elements using the adaptive meshing technique. We applied Dirichlet boundary conditions on the interface, that is, a uniform displacement has been applied on the compressing plate. We compressed the breast in the *y*-direction as shown in Fig 1. Zero displacements were set on the left vertical boundary plane of the breast model considering that the chest wall does not move during the breast compression. The plates are allowed to move only in the compressing direction, that is, in the *y*-direction.

The FEM breast geometry, explicitly, the node positions and their displacements under compression are used to simulate the x-ray mammographs assigning specific x-ray attenuation coefficients to the nodes. When x-ray photons pass through an object, they are attenuated due to the interaction of x-ray photons with the matter, mostly due to the photo-electric absorption and Compton scattering. Since the photo-electric effect and Compton scattering are dependent on the x-ray photon energy, the attenuation coefficient, which represent integral effects of those interactions, is also dependent on the photon energy. For the sake of simplicity, we assume here that x-rays are mono-energetic. Then, attenuation coefficient can be a function of space and represent by $\mu(\mathbf{r})$. The x-ray intensity passing through an object is expressed as:

$$I = I_0 \cdot e^{-\int_L \mu(\mathbf{r})dl} \tag{4}$$

where I is the intensity of the penetrated x-ray on the detector plane, I_o is the intensity of the incident x-ray to the object, L is the ray path through the object, and $\mu(\mathbf{r})$ is the linear attenuation coefficient at a position of $\mathbf{r}$.

With tissue deformation, the attenuation coefficient distribution, $\mu(\mathbf{r})$ also changes, hence, the x-ray projection image also changes. We calculate the projection images by simply obtaining the line integral of the attenuation coefficient:

$$\int_L \mu(\mathbf{r})dl = \ln \frac{I_0}{I} \tag{5}$$

If we assign x-ray linear attenuation coefficients to the heterogeneous breast FEM model, we can simulate the projection image of the object by ray tracing.

We have found from the literature [2] that the linear attenuation coefficients of fatty tissues are 0.3~0.8 1/cm while those of tumor tissues are 0.5~1.6 1/cm at the operating voltages of mammography. In the simulation settings, we consider the linear attenuation coefficients of background as 0.5 1/cm and for tumor tissue as 1 1/cm. Since biological tissues are virtually incompressible, we can assume that the linear attenuation coefficients of breast tissues do not change by the breast compression. The simulation of images and most of other soft computations in this study have been done using MATLAB (The MathWorks Inc., Massachusetts, USA).

Breast mimicking phantom and acquisition of experimental x-ray images

Phantoms with tissue mimicking properties are commonly used as a replacement of real tissue to validate or analyze a technique through experiment. We try to build a breast mimicking phantom with a tumor inclusion considering x-ray attenuation and elastic properties range of normal and tumor breast tissues. We also consider that the phantom has the capability of large recoverable deformation. The gel of the phantom has been produced dissolving poly vinyl alcohol (PVAL) in an equal mixture of ethanol and water. Differences in stiffness can be achieved using gels of varying poly vinyl alcohol concentration [14]. The mixture was heated to approximately 83 °C and stirred continuously till the PVAL fully dissolve. As ethanol evaporates during boiling, the heating was in close environment. We use 10% and 20% w/v PVAL mixture with equal ratio water and ethanol for background and inclusion respectively. The heating time was approximately 2 hours. Then the mixture was passed through 2 freeze and thaw cycles for 1 day in order to solidify it keeping the compressible nature. We solidified the inclusion first, and then, we placed the inclusion inside the poured liquid background material into a cup shaped mold and solidified it. The diameter of phantom was 5 cm and 4 cm for top and bottom side with a height of 6 cm. The inclusion was a 0.8 cm×0.8 cm×1 cm cube. The phantom looks transparent as shown in Fig. 2. The linear x-ray attenuation constant for 10% and 20% w/v PVAL mixture has average value of 0.77 1/cm and 0.85 1/cm respectively. The Young's modulus of this phantom varies with the increases of strain which, fortunately follows the nonlinear elastic theory and consequently shows its usefulness for breast mimicking phantom construction. The Young modulus for background and inclusion were varies 20~30 kPa and 100~250 kPa respectively for upto 20% strain. An acrylic frame was build to hold and compressed the breast phantom during x-ray imaging

as shown in Fig. 2. A movable plate has been used to compress the breast phantom with the help of screws. The x-ray imaging setup consists of a microfocus x-ray source (Hamammatsu L8121-01), a flat panel x-ray detector (Hamammatsu C7942SK-02) with 2240 by 2240 photodiode arrays and a columnar-structured CsI scintillator, and a rotation stage in between them [10]. The microfocus x-ray tube has a focal spot of 5~50 μm depending on the operating tube voltage and tube current. The tube setting for our experimental x-ray imaging was 60 KV and 250 μA.

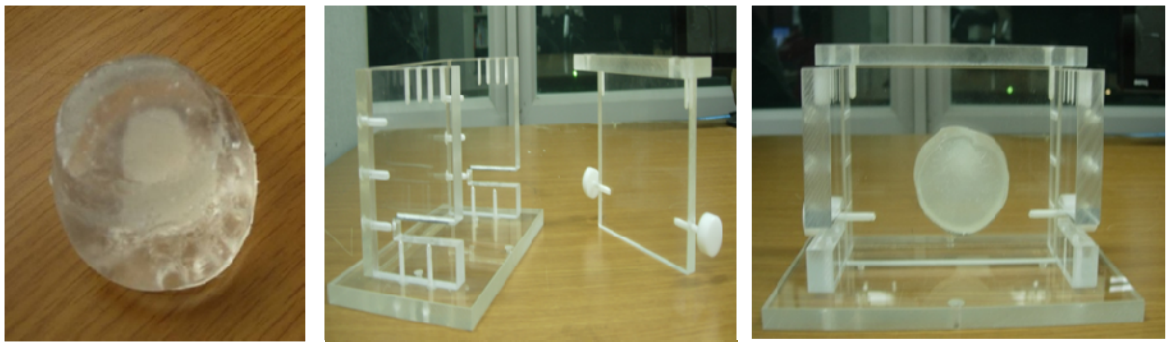

a) b) c)

Fig. 2 Experimental arrangement:
a) breast phantom, b) compression frame, and c) compressed phantom.

Results analysis and discussions

With the FEM analysis, we have calculated the displacements at the FEM nodes for three separate compression levels in axial directions. Fig. 3 shows the views of the mechanical deformation of the breast model under compression ratio of 15%, 20%, and 25% in terms of plate spacing. As the compressing plates squeeze the breast, the breast model is compressed in the vertical direction whereas it is expanded in the horizontal direction due to the incompressible nature of the breast tissues. There is a clear tendency that the softer background tissues are deformed more than the stiffer inclusions.

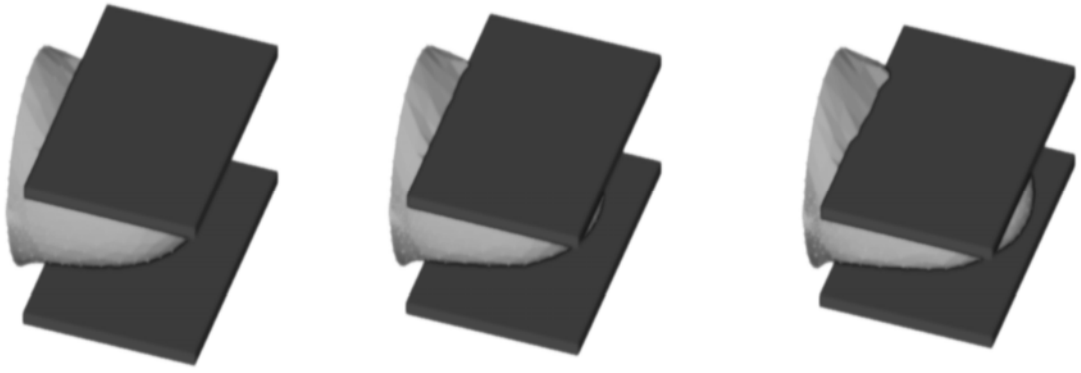

a) b) c)

Fig. 3 3D Deformation of the breast model under different compression levels:
a) 15% compression, b) 20% compression, and c) 25% compression.

We have simulated x-ray projection images of the deformed breast model taking into account the linear attenuation coefficients that were assigned to the breast tissues. In the calculation, we ignored the x-ray attenuation in the compressing plates and we assumed parallel x-ray

beam configuration for the sake of simple calculation. Fig. 4 shows the simulated x-ray projection images of the breast model under different compression ratios. From the projection images, we can see the expansion of the breast progresses in the horizontal direction.

We have taken x-ray radiographs under different compression steps. Fig. 5 shows the experimental radiographs with three separate compressions where Compression 1 < Compression 2 < Compression 3 with step of 5% of axial dimension starting from 15%. We plot the pixel intensity changes at the inclusions and surrounding region along a line as the contrast changes may not easily observed by visual inspection. Fig. 6 shows the intensity profiles comparison along a line passing through the inclusion. The obtained radiographs pixel intensities are negative of the detected x-ray intensity which mean that the more attenuation the brighter intensity.

We observed that between two compression level the intensity difference at background are bigger that the intensity difference in the inclusion. These differences in intensity change can induce additional contrast in mammograms. It is seen that the least compressed phantom image shows most brightness but the most compressed phantom image shows most contrast which is necessary to distinguish the inclusion from background.

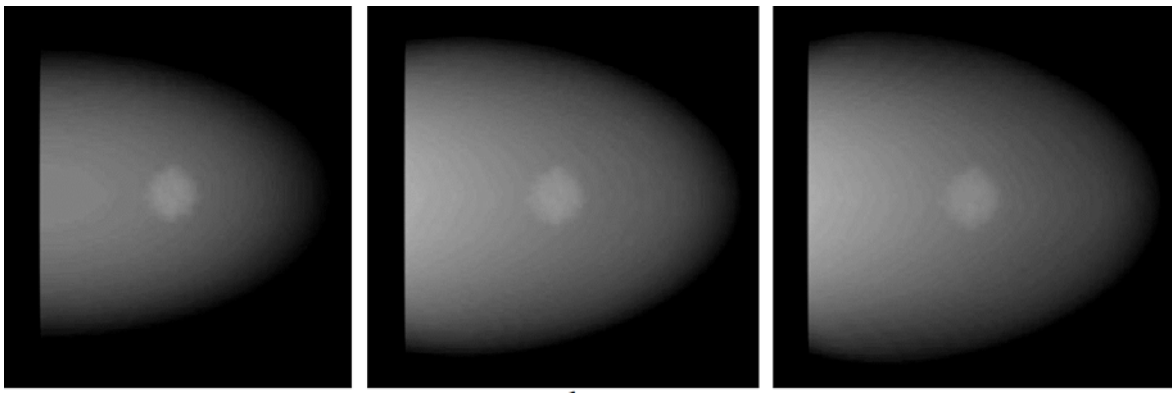

a) b) c)

Fig. 4 Simulated images of synthetic breast phantom under different compressions: a) 15% compression, b) 20% compression, and c) 25% compression.

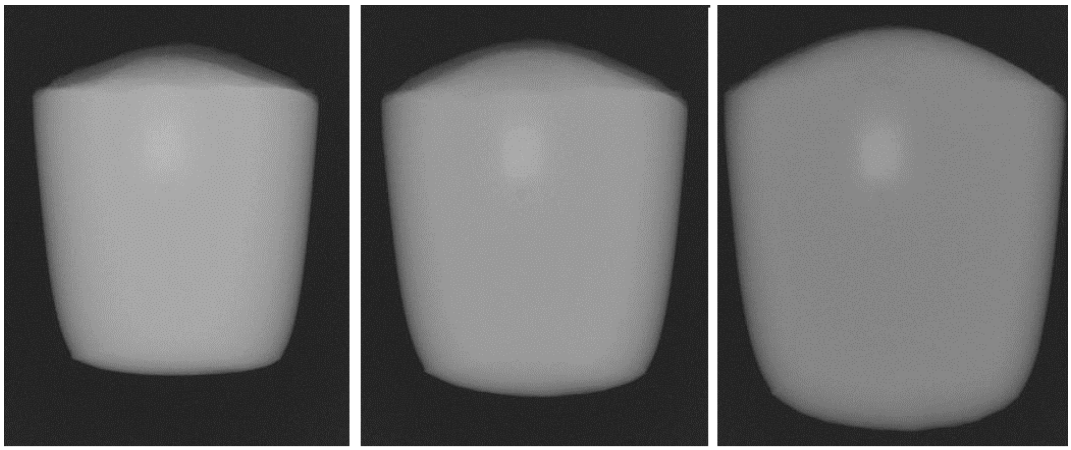

a) b) c)

Fig. 5 Experimental images of breast phantom under different compressions: a) 15% compression, b) 20% compression, and c) 25% compression.

In order to find the elasticity related intensity difference more accurately, we try to register a region of interest (ROI) with inclusion of the second step compression image to the similar ROI of the third step compression image. The second step compression ROI has been registered to third step compression ROI since the third step compression image has originally more contrast. We have used an intensity based non-rigid image registration where residual complexity is used as similarity measure [12]. This similarity measure has effectiveness in dense non-rigid registration, where the effects of nonlinear and slow-varying intensity distortions are more noticeable. The coding complexity of the residual image is measured instinctively in this method. The main strategy is that the residual (difference) image is expected to achieve the minimal complexity at the correct spatial alignment. Residual complexity is minimized according to the sparseness of the residual image using discrete cosine transform (DCT) basis. The gradient descent optimization method has been used for optimization. Due to the effectiveness of residual complexity as similarity measure for non-rigid registration of nonlinearly deformed images, we have chosen this method to register the compressed phantom radiographs.

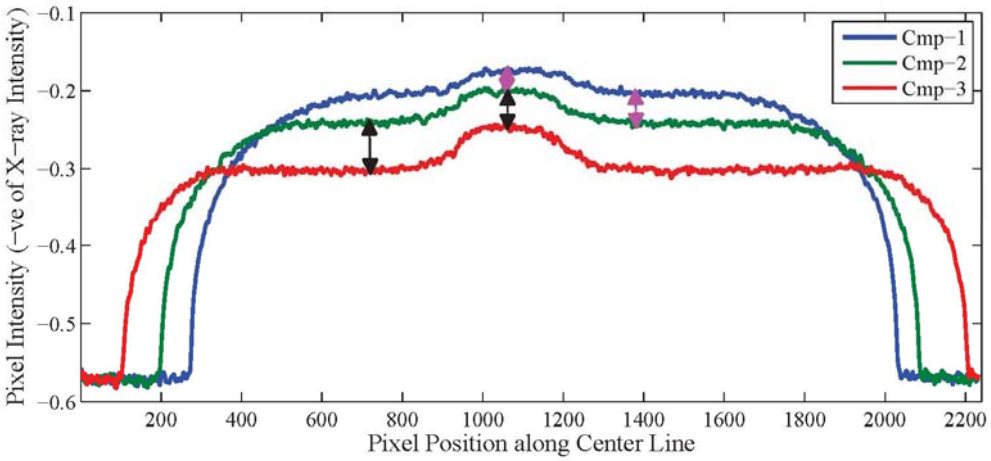

Fig. 6 Comparison of profiles along the center line
through inclusion under different compression steps

We have calculated the compression related contrast by subtracting the second step compression registered image from the third step compression (reference) image. This difference image has indicated that lower change in intensity in the inclusion region than that in background. To incorporate this contrast to the original image, intensity of each pixel of the difference image is reassigned by the subtracted value of mean intensity of difference image from the pixel intensity. Therefore, the values of pixel intensities become positive if they are greater than mean value and become negative if they are less than mean value. Finally, the modified difference image was added with the reference image to change its low intensities lower and high intensities higher. We also included a multiplying factor with the modified difference image during addition to see the impact of compression induced contrast.

Figs. 7 and 8 show contrast induced ROI along with the reference ROI of simulated and experimental images respectively. Each of these figures consists of reference ROI, compression induced contrast added ROI and compression induced contrast added ROI with a multiplying factor of 2. We have calculated difference of average pixel intensity of small rectangular regions inside the inclusion and in the nearby background to compare the contrast of obtained images. We have observed that the contrast was enhanced by a factor of about

1.4 and 2 for direct addition and addition with a multiplying factor of 2 respectively. The contrast improvement has also been visually justified from the Figs.7 and 8.

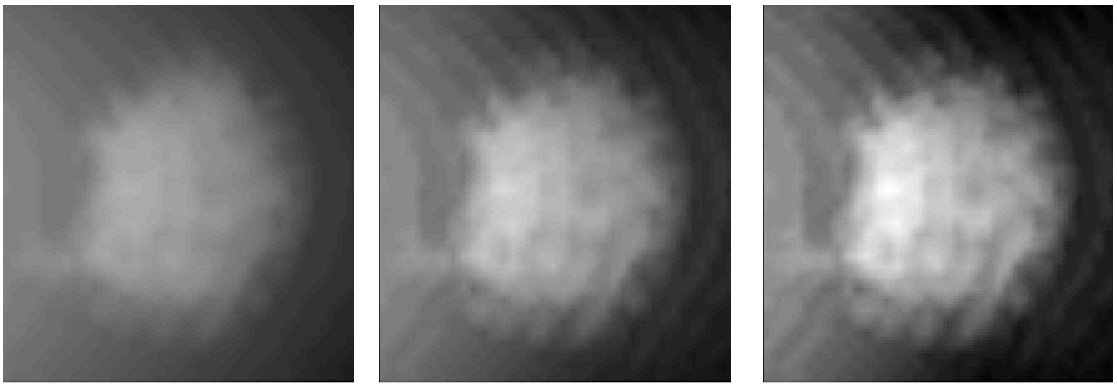

a) b) c)

Fig. 7 ROIs of simulated images:
a) reference ROI, b) compression induced contrast added ROI, and
c) compression induced contrast added ROI with 2 multiplying factor.

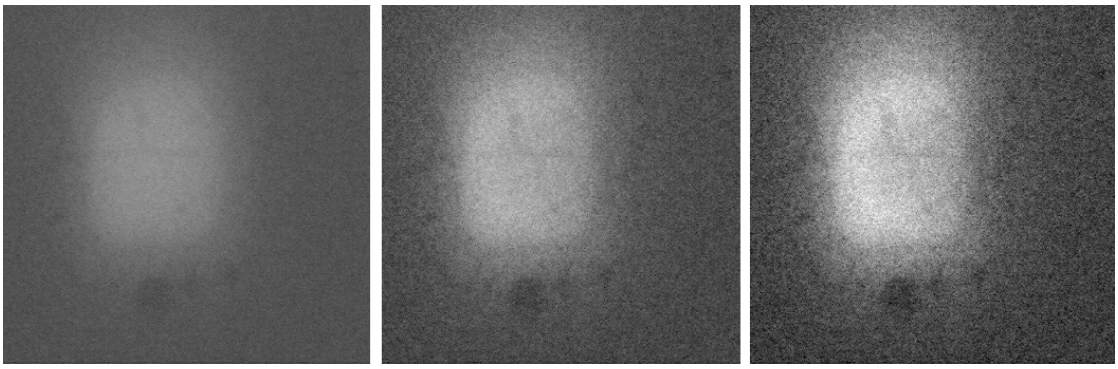

a) b) c)

Fig. 8 ROIs of experimental images:
a) reference ROI, b) compression induced contrast added ROI, and
c) compression induced contrast added ROI with 2 multiplying factor.

Conclusions

Additional contrast can be induced during the breast compression in x-ray mammography images owing to the different elasticity properties and x-ray attenuation between tumor and surrounding tissues. In this work, it has been studied that the pixel intensities at the tumor change more slowly than at the background due to small deformation of the tumor region. This compression related contrast can improve the original contrast of mammogram as found in this study. However, it may be awkward that the technique will need to take mammographic images at least two times with different compression levels. In support, this is usual practice in elastography. This study also has a limitation of using simple breast phantom rather than more realistic one which is useful for effective registration as well. We will try to develop more realistic breast phantom consisting fatty tissue, glandular tissue, cancerous tissue etc., which inescapably results in extra computational burden. We believe this groundwork study and its future progression will be helpful for clinical applications.

Acknowledgements

The financial support of this work was provided by the National Research Foundation of Korea (NRF) grant funded from the South Korea government (No. 2009-0078310).

References

1. Azar F., D. Metaxas, M. Schnall (2002). Methods for Modeling and Predicting Mechanical Deformations of the Breast under External Perturbations, Med Image Anal, 6, 1-27.
2. Chen R. C., R. Longo, L. Rigon, F. Zanconati, A. De Pellegrin, F. Arfelli, D. Dreossi, R. H. Menk, E. Vallazza, T. Q. Xiao, E. Castelli (2010). Measurement of the Linear Attenuation Coefficients of Breast Issues by Synchrotron Radiation Computed Tomography, Phys Med Biol, 55, 4993-5005.
3. Choy Y. H., W. T. Hung, R. A. Mitchell, X. Zhou (2007). An Automatic Statistical Method to Detect the Breast Border in a Mammogram, International Journal Bioautomation, 6, 38-48.
4. Ganesan K., U. R. Acharya, C. K. Chua, L. C. Min, K. T. Abraham, K.-H. Ng (2013). Computer-aided Breast Cancer Detection Using Mammograms: A Review, IEEE Reviews in Biomedical Engineering, 29, 155-171.
5. Holzapfel G. A. (2000). Nonlinear Solid Mechanics: A Continuum Approach for Engineering, Wiley.
6. Hossain A. B. M. A., M. H. Cho, S. Y. Lee (2011). Compression Induced Contrast Change in X-ray Mammogram: A Simulation Study, Biomedical Engineering Letters, 1, 49-55.
7. Hossain A. B. M. A., S. Y. Lee (2013). A Simulation Study on Strain Image Calculation from Digital Breast Tomosynthesis Data, Proc of 2nd Int Conf on Informatics, Electronics and Vision, Dhaka, Bangladesh, doi: 10.1109/ICIEV.2013.6572600.
8. Kim J. G., A. B. M. A. Hossain, J. H. Shin, S. Y. Lee (2012). Calculation of Strain Images of a Breast-mimicking Phantom from 3D CT Image Data, Medical Physics, 39, 5469-5478.
9. Krouskop T. A., T. M. Wheeler, F. Kallel, B. S. Garra, T. Hall (1998). Elastic Moduli of Breast and Prostate Tissues under Compression, Ultrasonic Imaging, 20, 260-274.
10. Lee C., H. K. Kim, I. K. Chun, S. Y. Lee, M. H. Cho (2003). A Flat-panel Detector Based Micro-CT System: Performance Evaluation for Small-animal Imaging, Phys Med Biol, 48, 4173-4185.
11. Lorenzen J., R. Sinkus, M. Lorenzen, M. Dargatz, C. Leussler, P. Rochmann, G. Adam (2002). MR Elastography of the Breast: Preliminary Clinical Results, RöFo-Fortschritte auf dem Gebiet der Rötgenstrahlen und der Bildgebenden Verfahren, 174, 830-834.
12. Myronenko A., X. Song (2010). Intensity-based Image Registration by Minimizing Residual Complexity, IEEE Trans Med Imag, 29, 1882-1890.
13. Ophir J., S. K. Alam, B. Garra, F. Kallel, E. Konofagou, T. Krouskop, T. Varghese (2002). Elastography: Imaging the Elastic Properties of Soft Tissues with Ultrasound, J Med Ultrasonics, 29, 155-171.
14. Price B. D., A. P. Gibson, L. T. Tan, G. J. Royle (2010). An Elastically Compressible Phantom Material with Mechanical and X-ray Attenuation Properties Equivalent to Breast Tissue, Phys Med Biol, 55, 1177-1188.
15. Samani A., D. B. Plewes (2007). An Inverse Problem Solution for Measuring the Elastic Modulus of Intact Breast Tissue Tumours, Phys Med Biol, 52, 1247-1260.

16. Samani A., J. Zubovits, D. B. Plewes (2007). Elastic Moduli of Normal and Pathological Human Breast Tissues: An Inversion-technique-based Investigation of 169 Samples, Phys Med Biol, 52, 1565-1576.
17. Wang Z. G., Y. Liu, G. Wang, L. Z. Sun (2008). Elasto-mammography: Elastic Property Reconstruction in Breast Tissues, AIP Conference Proceedings, 973, 209-215.

Assoc. Prof. A. B. M. Aowlad Hossain, Ph.D.
E-mail: aowlad0403@ece.kuet.ac.bd

Dr. A. B. M. Aowlad Hossain received his B.Sc. in Electrical and Electronic Engineering (EEE) from Khulna University of Engineering & Technology (KUET) and M.Sc. in EEE from Bangladesh University of Engineering & Technology (BUET) in 2002 and 2005 respectively. He joined KUET as a lecturer in 2005. A. B. M. A. Hossain completed his Ph.D. in Biomedical Engineering from Kyung Hee University, Korea in 2012. Currently he is an Associate Professor in the Department of ECE, KUET. His research interests are ultrasound imaging, ultrasound and x-ray elastogarphy etc. He is a member of different professional societies and a reviewer of different conferences and journals.

Prof. Min Hyoung Cho, Ph.D.
E-mail: mhcho@khu.ac.kr

Professor Min Hyoung Cho has obtained M.Sc. and Ph.D. in Electronic Engineering from Korea Advanced Institute of Science and Technology (KAIST) in 1985 and 1990 respectively. Then he joined Samsung Advanced Institute of Technology as a Senior Researcher. He was an Assistant and a Associate Professor in University of Suwon from 1992 to 2000. Currently, he is working as a Professor in the Department of Biomedical Engineering of Kyung Hee University. His research areas of interests are medical imaging, medical signal and image processing etc. He is a member of different professional societies and reputed journal editorial committees.

Prof. Soo Yeol Lee, Ph.D.
E-mail: sylee01@khu.ac.kr

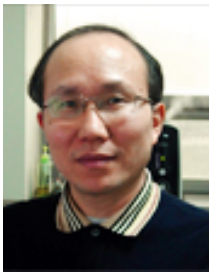

Soo Yeol Lee is working as a Professor in the Department of Biomedical Engineering of Kyung Hee University from 1999. He has obtained M.Sc. and Ph.D. in Electronic Engineering from KAIST in 1985 and 1989 respectively. He has started his career in Samsung Electronics as R&D Engineer. He was an Assistant and an Associate Professor in Konkuk University, Korea from 1992 to 1999. His research areas of interests are MRI, micro-CT, infrared imaging device, bio-signal processing, elastographic imaging, etc. He is a member of different professional societies and reputed journal editorial committees.